8500 *Macromolecules* **2009**, *42*, 8500–8512
DOI: 10.1021/ma9014438

Macromolecules
ARTICLE

Confined Sphere-Forming Block Copolymers: Phase Behavior and the Role of Chain Architecture

G. J. A. Sevink*,† and A. V. Zvelindovsky‡

†*Leiden Institute of Chemistry, Leiden University, PO Box 9502, 2300 RA, Leiden, The Netherlands, and* ‡*Computational Physics Group, University of Central Lancashire, Preston PR1 2HE, U.K.*

Received July 3, 2009; Revised Manuscript Received August 27, 2009

ABSTRACT: We have considered the phase behavior of sphere-forming block copolymers in confinement by means of dynamic density functional theory (DDFT). We have in particular focused on the role of the chain architecture by choosing two equivalent AB and ABA block copolymers. The role of surface fields (ε_M) and film thickness (H) on the phase behavior is elucidated. For both systems, we identified surface reconstructions such as a wetting layer, parallel cylinders, perforated lamellae and lamellae, that were previously also found in confined cylinder-forming systems. In contrast to cylinder-forming systems, we observed that the part of the film that is affected by the surface field depends on the nature of the surface layer. In particular, cylindrical and lamellar surface reconstructions connect to the bulk structure in the interior of the film via cylindrical layers. The origin of this extended surface field range lies in the restricted chain conformations. As a direct consequence, confinement plays a role also in relatively thick films for stronger surface fields. We show in detail the complex interplay between the surface field and confinement, and how this introduces a certain amount of asymmetry even for this setup with symmetric wetting conditions. We identified the role of the chain architecture, which is only striking in "neutral" surfaces, where a small repulsive interaction balances the entropic gain of positioning the shortest block next to the surface. The AB diblock forms a layered spheres structure for most H, while for the ABA triblock a new structure, perpendicular cylinders that span the film, is observed for all considered H.

1. Introduction

Ordered fluids like amphiphilic AB or ABA block copolymers tend to self-assemble into ordered microstructures with characteristic lengths determined by the molecular size, i.e., in the 10−100 nm range.[1] The microdomain structure in the bulk is determined mainly by the molecular architecture, in particular the ratio of block lengths, and the interaction between the two components. In thin films an additional driving force for structure formation exists, because one component typically has a lower interfacial energy than the other. Numerous studies have dealt with thin films of lamella-forming block copolymers and two major effects have been identified.[2] Preferential attraction of one component to the surface (the surface field) causes lamella to align parallel to the surfaces and the film forms islands and holes where the film thickness is a (half) integer multiple of the lamella spacing in the bulk. In cases where the film thickness is incompatible with the natural domain spacing (the incommensurable situation), or when the surfaces are not selective, the block copolymer chains align along the confining surface and lamellae perpendicular to the surfaces are formed.

In analogy to surface reconstructions of crystal surfaces, the near-surface structure in block copolymers can also deviate from the bulk structure.[3] Lamella-forming block copolymers represent a special class in this respect, as parallel lamellae exhibit the same symmetry as the confining planar surface. Recent experimental studies for cylinder-forming block copolymers have indeed observed that considerable rearrangements of microdomains near the surface are possible.[4−8] Detailed modeling (see ref 9 for a summary) and combined experimental/modeling studies[10,11] corroborated that, although this effect is sensitive to several internal factors, it is *universal* and not specific to a certain system or route of film preparation. A general feature is that an increasing surface field leads to *surface reconstructions*, i.e., stabilization of parallel structures with increasing planar symmetry or decreasing overall mean curvature, such as perforated lamellae (PL) and lamellae (L). For the system considered in our earlier publications,[10,11] surface reconstruction was restricted to the vicinity of the confining surface, quantified as the *range* of the surface field. This range, which depends on the system parameters in a nontrivial way, was determined as roughly one domain spacing. In the interior of the film, the structure has a layered character but remained (bulk) cylindrical. A recent experimental study of Park et al. indicates that this range can be larger.[12] In supported thin films of a cylinder-forming PS-*b*-PMMA block copolymer they found PL surface reconstructions that extend much deeper into the film, up to 6 layers of structure. They mention that this observation is highly unexpected and that further theoretical investigation is required.[12] Here, we only note that the possible finding of an increased surface field range does not affect the general description.

For thin films of fixed thickness (slits) or on the slopes in supported films, incommensurability of the natural domain spacing and the film thickness modulates the stability regions of the parallel structures and cause easier deformable phases, i.e., phases associated with reduced elastic chain deformation, to occur at intermediate film thicknesses. In particular, for weak surface fields, incommensurability gives rise to perpendicular instead of parallel cylinders and, for stronger surface fields, to phases with an increasing overall curvature. For very thin films, incommensurability can even prevent microphase separation.

*Corresponding author. E-mail: a.sevink@chem.leidenuniv.nl.

 Published on Web 09/11/2009

In combination, the surface field and incommensurability cause a complex and interesting phase behavior.

In confined lamellar- and cylinder-forming systems, parallel microdomains span the films in at least one direction, *enabling* control along this direction. This property is not intrinsic for sphere-forming systems, and, in addition, spherical morphologies are more difficult to image in detail. These systems were first studied experimentally by Henkee et al.,[13] who considered structure formation in thin film droplets of poly(styrene butadiene) diblock copolymer in detail. The surface geography in the thicker part of the droplet was found to reflect the underlying structure, i.e., layers of hexagonally packed spherical micelles, and therefore it exhibits surface steps of pronounced thickness. An offset between adjacent hexagonally packed layers, originating from the requirement to fill interstitial space, was identified but apart from this offset the layers were found to stack randomly. Although the term was introduced later, they also observed a surface reconstuction and explained it in terms of surface energetics, in particular the preferential segregation of one of the blocks to the surface. The surface reconstruction, a featureless region of constant thickness, was found in the thinnest peripheral region of the droplet. Although there was some evidence for a few very poorly developed spherical microdomains in the interior area of this peripheral region, it was characterized by uniformity in image contrast, i.e., an unstructured wetting layer.[13] On the basis of this pioneering work and the requirement of neat structures for nanotechnology, most later studies have focused on *packing of spherical domains*, in particular obtaining neat structures on a larger scale and on the nature of the transition from a hexagonal (*hex*) structure in very thin (2D) films to the 3D (*bcc*) bulk lattice upon increasing the film thickness.[14−19] Detailed experiments and theory corroborated that the in-plane order changes from *hex* to *bcc* via an abrupt (between 4 and 5 layers) transition to orthorhombic. Upon further increasing the thickness the orthorhombic in-plane order asymptotically approaches the *bcc* symmetry (110 plane). The fundamental role of surface reconstruction in sphere-forming systems is much less clear. In the past, several types of external fields (electric fields[20,21]) and applied steady shear[22] have shown to induce order-to-order (OOT) transitions from spheres to cylinders. In addition to lamellar surface reconstructions, cylinders were also found in confined sphere-forming systems.[23−25] Intuitively, one could consider surface reconstructions in cylinder-forming systems as a subset of possible surface reconstructions in sphere-forming systems, but this assumption should be considered in detail. A fundamental understanding of surface reconstructions and the role of confinement on their stability is currently lacking.

Our particular interest in confined sphere-forming systems was not only triggered by this lack of fundamental understanding, but also by experimental observations in the group of Kramer.[26] Upon comparing SEB (diblock) and SEBS (triblock) thin films by AFM and GISAXS the surface structure in the diblock was found to change from dots to stripes, upon variation of the substrate (polystyrene brush or silicon oxide) or the film thickness. The triblock system always shows dots, regardless of these experimental conditions. In addition, scattering experiments indicate that dots represent spheres instead of perpendicular cylinders. In both systems, the structure remains unaffected when the films are annealed above or below the bulk OOT (from spheres to cylinders). Different cooling rates have an effect on the surface structure in both di- and triblock systems. Since these film are intrinsically multiscale systems, subject to competition between microphase separation and terrace formation, the overall behavior is complex and detailed investigation is required to unravel different factors. We note that the experimental data has not been published and that the data available to us is not decisive in this respect. As the origin can be either kinetic or thermodynamic, a theoretical treatment of both factors is valuable. In addition, we have previously shown for a cylinder-forming SBS system[10] how a stepwise procedure, i.e. stepwise increasing the complexity from thin slits with symmetric wetting conditions,[10,11] thin slits with asymmetric wetting conditions,[27] and dynamics of a phase transition in slits with changing surface field[28] to terrace formation[29,30] and defect dynamics in supported films[31,32] can be valuable for the understanding and analysis of the fundamental processes in experimental substrate-supported films.

Here, we focus on the first step and consider structure formation in sphere-forming systems confined in thin slits, using symmetric wetting conditions. We use the same DDFT treatment that was previously applied for cylinder-forming systems. We focus on thermodynamic factors, the role of chain architecture, by considering two equivalent systems, denoted by AB (diblock) and ABA (triblock). Kinetic factors are natural in our approach, as our minimization of the free energy is based on a (diffusive) kinetic model. The universality principle, i.e. the general behavior in confinement is determined by the structure *type* in bulk and not by specificity,[10] is exploited by using a ABA reference system taken from earlier studies. In particular, we consider the ABA system in the part of phase space where spheres are stable, closer to the OOT (from spheres to cylinders) than to the order-to-disorder transition (ODT).[29] As the elastic chain deformations are sensitive to the relative 'distances' to phase boundaries (ODT and OOT), we have carefully calibrated the AB system to this reference system. Analogous to our previous studies, we elucidate the fundamental factors that determine the behavior in confinement.

2. The DDFT Model

We describe the model only briefly (for details, see ref 33). We model the polymer film as a collection of Gaussian chains, each representing a copolymer molecule in a mean field environment. The chain is build from coarse-grained statistical units or beads with general architecture $A_{N_A}B_{N_B}C_{N_C}...$ and length $N = \Sigma_I N_I$. Different bead species denote different chemical entities or blocks. In experiments, films are often prepared on a solid substrate and terrace formation is an important phenomena for avoiding structure frustration due to incommensurability. We note that information about this effect can in principle be deduced from slit calculations,[34] and that the thickness profile in the experimental film is continuous. For this reason, the polymer is confined between two parallel solid surfaces in our setup. The free energy functional has the form[33]

$$F[\rho] = -kT \ln \frac{\Phi^n}{n!} - \sum_I \int_V U_I(\mathbf{r})\rho_I(\mathbf{r})\, d\mathbf{r} + F^{nid}[\rho] \quad (1)$$

where V is the system volume, n is the number of polymer molecules in V, Φ is the intramolecular partition function for ideal Gaussian chains, and I the block type index. The external potentials U_I are conjugate to the densities or concentration fields ρ_I via the Gaussian chain density functional[35]. Confinement is represented by a so-called stationary mask field ρ_M. The nonideal term F^{nid} includes two terms representing the mean-field interactions between the different ρ_I as well as a Helfand penalty term for incompressibility of the total system.[33] In line with our earlier work, the interactions are specified by the parameters ε^0_{IJ} (in kJ/mol),[36] which are directly related to the dimensionless Flory−Huggins parameters by $\chi_{IJ} = \varepsilon^0_{IJ}/n_A k_B T$ (with n_A Avogadro's number, k_B the Boltzmann constant, and $T = 300$ the temperature in Kelvin). Since all interactions terms consider a local Gaussian interaction kernel, the surface field[10] is relatively short ranged. However, distances further away from the surfaces

are affected due to the connectivity of the chains. In spirit of our previous work the free energy functional F is minimized in a dynamic fashion. The time evolution of the density fields is described by a Landau−Ginzburg type of diffusion equation[35]

$$\frac{\partial \rho_I}{\partial t} = M_I \nabla \cdot \rho_I \nabla \mu_I + \eta_I \tag{2}$$

with M_I the mobility of the different block types, μ_I are the chemical potentials with proper boundary conditions at the interfaces,[33] and η_I a noise field that satisfies the fluctuation−dissipation relation.

3. System and Parametrization

In an earlier study, we used the triblock $A_3B_{12}A_3$ to study the effect of applied electric fields in sphere-forming systems. In this system, spheres are stable in bulk for $5.8 \leq \varepsilon^0_{AB} \leq 6.0$. In thin slits, we found two different mechanisms for the transition of spheres into standing cylinders $C_\perp$ upon application of an electric field above some threshold strength. For $\varepsilon^0_{AB} = 5.8$ spheres transform to cylinders via a detour in disorder and for $\varepsilon^0_{AB} = 5.9$ the spheres merge to form cylinders in a direction that is dictated by proximity. Here, we consider the triblock system with $\varepsilon^0_{AB} = 5.9$, closest to the bulk OOT for spheres to cylinders, as a reference system. We denote this interaction strength as ε^{tri} in the remainder. Previously, we have used the same triblock, for $\varepsilon^0_{AB} = 6.5$, to study the behavior of an experimental SBS system in confinement. This system forms cylinders in the bulk. Both A_6B_{12} and A_3B_6 are natural candidates for the equivalent diblock system, and we consider A_3B_6 that give rise to equal domain sizes ($f_A = N_A/N = 1 - f_B = 1/3$). The equivalent interaction strength ε^0_{AB} for the diblock system is not necessary the same as for the triblock system due to the different and finite length of the chains. We will determine this interaction strength for the diblock ε^{di} in detail in the next section. The other parameters for the diblock and triblock systems are equal. Excluded volumes and mobilities are the same for all bead types, $M_I = M$ and $\nu_I = \nu$. The dimensionless time step was set to $\tau = M\Delta t/h^2kT = 0.73$.[37] The parameter h is the grid distance between two neighboring nodes in the computational grid of total size $L_x \times L_y \times H + 2$, where H is the film thickness (in h). In the vicinity of surfaces rigid wall boundary conditions are used,[33] and periodic boundary conditions in all Cartesian directions where no wall is present. All calculations were started from the same initial condition (unless mentioned otherwise), corresponding to uniform density distributions (complete mixing) with external fields $U_I = 0$. Most of the stable structures were obtained by the numerical integration procedure (2) using 5000 dimensionless time steps. Stability was monitored using the free energy and the order parameter P,[35,38] and in some cases additional time steps were used until no significant changes were observed. Both the film thickness H (in h) and effective surface interaction $\varepsilon_M = \varepsilon_{AM} - \varepsilon_{BM}$ (in kJ/mol) were varied with integer increments. These effective surface interactions ε_M were previously introduced,[33] due to the observation that only the difference matters in the calculation of the chemical potential. In all cases, the term "neutral" refers to the ε_M for which the weak repulsion of the A block levels with the entropic gain of positioning the shortest A part next to the surface; it will be used rather freely. In the slit calculations, the density fields $\rho_A(\mathbf{r})$, associated with the sphere-forming block, were visualized by an isosurface (for isovalue $\nu\rho_A(\mathbf{r}) = 0.5$) and classified by visual inspection.

4. Determining the Diblock Interaction Parameter

We determine the equivalent ε^{di} for the diblock system based on a similarity measure for the (quasi)equilibrium structures. We first determine the phase behavior for the diblock system ($f_A = 1/3$, $N = 9$). Previously, self-consistent field theory (SCFT)[39] for AB diblock copolymers showed that disorder, spheres, cylinders, gyroid and lamellae are the only stable structures, and that they are found in this order for $f_A = 1/3$ upon increasing χN.

4.1. Bulk Phase Behavior. We determine the bulk diagram of A_3B_6 for a $32 \times 32 \times 32$ computational grid, using increments of $\Delta\varepsilon = 0.05$, based on the dynamic equation 2. In determining the equilibrium bulk behavior using DDFT and varying χN, several biases can be identified that either originate from limitations of the model or the use of computational volumes of fixed size. First, composition fluctuations can become significant in the vicinity of the order−disorder transition, in particular for low molecular weights.[40,41] Mean-field descriptions like the one used here do not account for fluctuations, and are therefore less accurate for finite chains in very weak segregation. In particular, the Landau expansion of the SCFT of Leibler[42] for diblocks predicts a first order phase transition to *bcc* (spheres) for $f_A \neq 0.5$ on increasing χN from the homogeneous melt, and moreover that, upon further increase, a transition from *bcc* to hexagonal (cylinders) and subsequently to lamellae is possible. Incorporating fluctuation corrections to this theory not only shifts the phase boundaries but shows that also direct transitions from the homogeneous melt to cylinders or lamellae are possible.[40] We note these findings, but consider our DDFT approach, based on the SCFT free energy, sufficient for our purpose. We do not focus on peculiarities like exact locations of phase boundaries, but rather on a unifying picture for equivalent systems. Second, we note that the driving forces for phase separation in our diffusive model are very small in the considered regime. The noise that is added at each time step (TMS) can easily disrupt the cooperative transfer of material that is required for structure formation, and suppress phase separation. Third, the periodic boundary conditions serve as an additional constraint, and give rise to an artificial free energy contribution F^{bound} due to the imposed structure periodicity. Owing to the ability of the system to distribute mismatches over larger structures, this boundary term will decay with increasing volume. However, since the *bcc* phase constitutes optimal 3D packing[43−45] this "soft" crystal will in general experience much larger frustration than a 2D soft crystal such as cylinders due to the boundary conditions along the three principal axes. The same holds for space-spanning bicontinuous structures like gyroid. In particular, hexagonally packed cylinders can reorient as a whole to fit the calculation volume without altering the chain conformations within cylinders. A solution for this general problem was originally formulated for molecular dynamics, and is aimed at minimizing F^{bound} via a pressure term that considers the calculation volume as an adaptive parameter.[46] Although the idea is very simple, implementation is much harder in our case, since a/h, the ratio of the bond-length a and grid distance h, is fixed for numerical reasons.[47] Instead, we resolve these issues by a set of additional calculations using 'artificial' dynamics in a fixed volume.[48] This Picard scheme, developed as a tool for combinatorial screening of self-assembly, is given by

$$\frac{\partial \rho_I}{\partial t} = D_I \mu_I + \eta_I \tag{3}$$

with D_I a scaling parameter and η_I is noise that is added to guide the system over small energy barriers. The deterministic part of (3) is a general iterative minimization procedure to obtain the stationary solution $\mu_I = 0$. Owing to the lack of

gradients, this method allows for nonlocal mass transfer and faster equilibration.

Using diffusive dynamics (eq 2) for TMS = 5000, we identified the following bulk structures based on visual inspection: $\varepsilon^{di} \leq 6.45$, disorder; $6.5 \leq \varepsilon^{di} \leq 6.6$, spheres; $6.65 \leq \varepsilon^{di} \leq 6.8$, cylinders or coexisting spheres/cylinders; $6.85 \leq \varepsilon^{di} \leq 6.9$, coexisting cylinders/gyroid; $6.95 \leq \varepsilon^{di} \leq 7.0$, gyroid. The earlier mentioned effects give rise to uncertainty in the assignment of stable phases and phase boundaries. Examples are the coexisting structures, the absence of genuine *bcc* ordering in the sphere structures and very defected gyroid structures. Consequently, we used the spheres obtained for $\varepsilon^{di} = 6.55$ as a starting structure for the Picard scheme and monitor the evolution of the free energy until a plateaux is reached. This procedure resolves the kinetic factor and we find: $\varepsilon_{di} \leq 6.4$, disorder; $6.45 \leq \varepsilon^{di} \leq 6.6$, spheres; $6.65 \leq \varepsilon^{di} \leq 6.7$, coexisting spheres and short cylinders; $6.7 \leq \varepsilon^{di} \leq 6.85$, cylinders; $6.9 \leq \varepsilon^{di} \leq 7.0$, gyroid. In the range 6.65−6.7, the free energy is very noisy over the full TMS = 20000 and decreases only very slowly on average. Application of the Picard algorithm starting from perfect cylinders in this range gives a lower free energy; the initial cylindrical structure slowly reorients as a whole via cylinder breakage and reconnections. These results indicate that the free energy difference between spheres and cylinders is small, and in particular that the F^{bound} associated with *bcc* is roughly comparable to this difference.

4.2. Similarity Measure. We use a measure based on a unique description of structural properties in terms of shape and connectivity of patterns formed by pixels of binary 3-D images.[38] Minkowski functionals $W_\nu(\mathscr{P})$ (ν = 0, 1, 2, 3) describe the morphological information contained in an image $\mathscr{P}$ by numbers that are proportional to very simple geometrical and topological quantities: the volume V, the surface area S, the mean curvature H, and the Euler characteristic χ. This family of Minkowski functionals (MF) forms a complete system of morphological measures on convex bodies, in the sense that any image functional with similar properties can be written as a linear combination of these MFs. The initial step in the analysis is the generation of black-and-white pictures with black pixels representing the object, and white pixels the background. In particular, the picture $\mathscr{P}(h)$ is constructed from the dimensionless reference field $\theta(\mathbf{r}) = \nu\rho(\mathbf{r})$ as

$$\mathscr{P}(h, \mathbf{r}) = f(\theta(\mathbf{r}) - h) \tag{4}$$

where $f(x)$ is the Heaviside step function (0 or 1) and h is a threshold in [0,1]. The set of Minkowski functionals $\{W_0, W_1, W_2, W_3\}$ for an image $\mathscr{P}(h)$ are calculated using the method described in ref 38. We find distinct signatures for the diblock systems in the target range $6.5 \leq \varepsilon^{di} \leq 6.7$, enabling the construction of a measure based on all four MFs without any scaling. Introducing $\mathscr{P}^{tri}(h)$ as the picture representing the shortest block in the triblock structure ($\varepsilon^{tri} = 5.9$) and $\mathscr{P}^{di}(h)$, the equivalent diblock picture for varying ε^{di} (both at TMS = 5000), we introduce a distance measure

$$d(\varepsilon^{di}) = \sum_{\nu=0}^{4} ||(W_\nu(\mathscr{P}^{tri}(h)) - W_\nu(\mathscr{P}^{di}(h))|| \tag{5}$$

with $\|\cdot\|$ being the (discrete) l^2 norm. We have discretized [0,1] using $\Delta h = 0.002$. In Figure 1, we plot the distance measure d for varying interaction ε^{di}. From this figure, one observes that the diblock structure obtained for $\varepsilon^{di} = 6.55$ is equivalent to the structure obtained for the triblocks in terms of structural properties. Closer comparison of $W_3(h)$ ($\sim H$) and $W_4(h)$ ($\sim\chi$) for both tri- and diblocks for this value (see Figure 2) reveals that the signatures of the curves are very similar and that the locations of the extrema are well-reproduced. We use this value $\varepsilon^{di} = 6.55$ in the remainder, but first determine the equilibrium distance s_0 between layers of spheres. A perfect *bcc* lattice of spheres is obtained in a 34^3

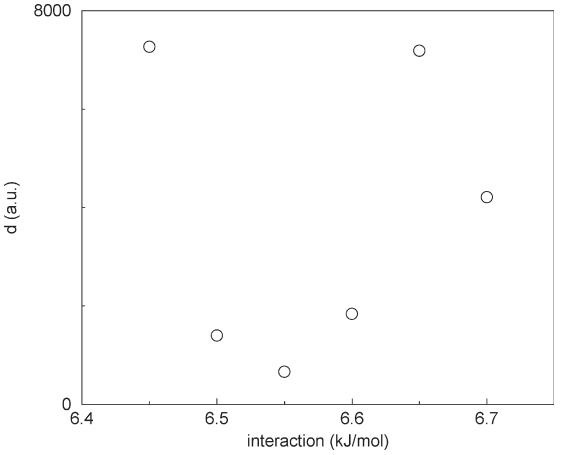

Figure 1. Distance measure d for varying ε^{di}. The considered computational volume was $L_x \times L_y \times L_z = 32 \times 32 \times 32$. The discretization distance for the threshold $h \in [0,1]$ used in the MF calculation was $\Delta h = 0.002$.

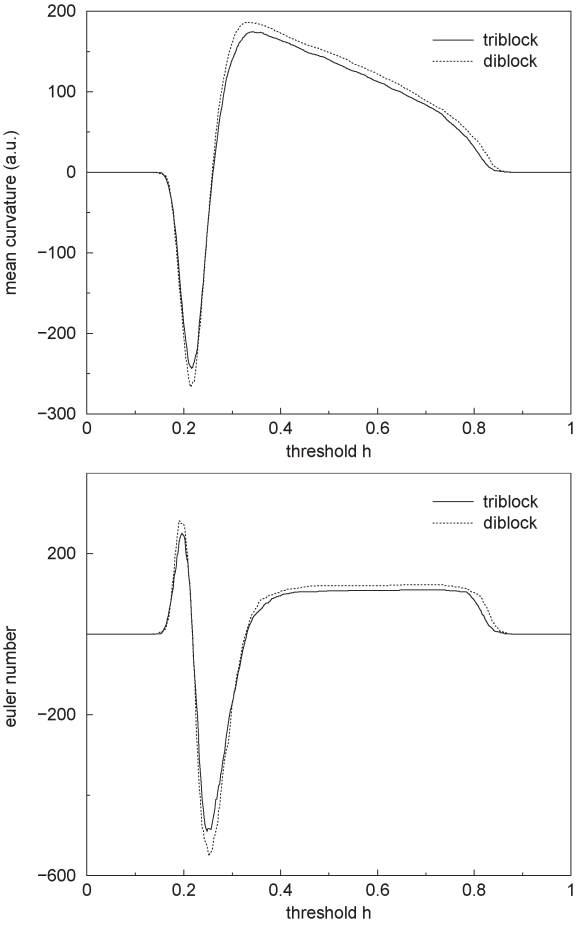

Figure 2. The integrated mean curvature and euler characteristics for varying threshold h, using $\Delta h = 0.002$. Solid line: MF for the triblock system with $\varepsilon = 5.9$. Dashed line: MF for the diblock system, using the optimal $\varepsilon = 6.55$ determined based on the distance measure in Figure 1.

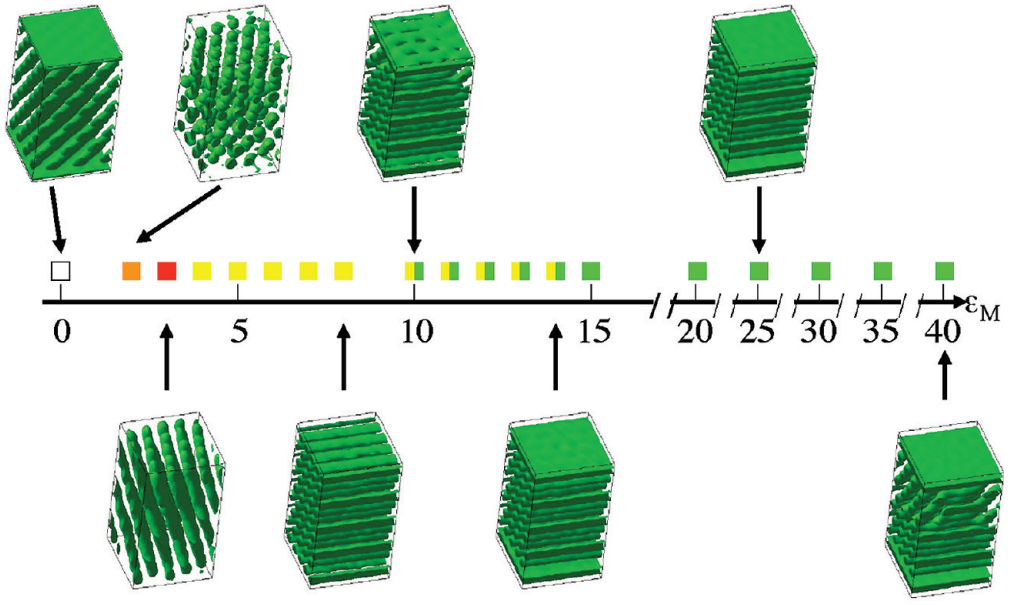

Figure 3. Stable structures in relatively thick films for the ABA triblock and $\varepsilon_{AB} = \varepsilon^{tri} = 5.9$. The film thickness $H = 54$ is constant and the surface field ε_M varied. The free energy was monitored during structure evolution, and calculations where extended when the free energy did not reach a constant value within 5000 steps. Representative structures are shown, and arrows indicate their location on the phase line. Colors denote the structure in the surface layers. The value used for generating the isosurfaces was the average value.

volume. To derive an initial guess for the domain distance s_0 in confinement, we use the suggestion that thin films adopt the *bcc* lattice with the closest-packed (110) plane oriented parallel to the confining surfaces. The distance s_0 between layers containing hexagonally arranged spheres is thus determined as 5.8 gridpoints.

5. Results

We now turn to confinement: what happens when surfaces are added to the systems? We consider and compare the effect of film thickness, H, and strength of the surface field, ε_M, on the structure formation in two systems: $A_3B_{12}A_3$ for $\varepsilon^{tri} = 5.9$ and A_3B_6 for $\varepsilon^{di} = 6.55$. We refer to the first as "triblock" and the second as "diblock". Generally speaking, the presence of surfaces has several effects. The reduced configurational entropy in the vicinity of the confining surfaces (symmetry breaking) leads to accelerated microphase separation when compared to the bulk. Phase separation starts close to the surfaces and propagates into the bulk of the film. As a result, this initial structure will at first adapt the planar symmetry of the confining surface, and at later stages rearrange according to the thermodynamic driving forces. The formation of structures with long-range order is therefore enhanced.[11] The surface energy, i.e. the interaction of the block with the surface, is also very important. Depending on the difference in surface energy ε_M, chains will align perpendicular ($\varepsilon_M > 0$) or parallel to the surface ($\varepsilon_M \approx 0$), and *parallel* or *perpendicular* structures will be stable, respectively. When $f_A \neq 1/2$, there is an entropic penalty for positioning the longest block next to the surface, leading to a shift of perpendicular structures to nonzero ε_M.[11] A very intriguing effect are deviations from the bulk microdomain structure in the vicinity of the interface or so-called surface reconstructions. This effect is caused by the large energetic penalty for the least favored block to be located in the vicinity of the surface when ε_M is above some threshold value. All these effects are modulated by the chain architecture, as the triblock can form both "loops" and "bridges", and by confinement. In particular, packing constraints resulting from the natural domain distance and the thickness H can lead to very complex behavior.

5.1. Notation and Color Scheme. In the remainder, we consider all factors in detail and use the symbolic notation that was developed in refs 10 and 11 to denote structures. The boxes in the structure diagrams represent stable structures obtained by DDFT after finite simulation time. We use the following standard color scheme: wetting layer (W), white; disorder (D), gray; spheres (S), orange; perpendicular cylinders ($C_\perp$), red; parallel cylinders ($C_\parallel$), yellow; perforated lamellae (PL), blue; lamellae (L), green. Two-colored boxes indicate that two phases associated with these colors coexist after the finite simulation time.

6. Surface Reconstructions

We focus on *surface reconstructions* by considering relatively thick films. We have previously shown that for cylinder-forming systems[10,11] the two important factors, surface field and confinement, are decoupled in thick films, since mismatches of the natural domain spacing and the slit thickness H can be distributed over several layers. Moreover, due to large separation between the two confining surfaces, in the vicinity of one surface the influence of the other one is negligible. In Figures 3 and 4, we show the structures obtained for the triblock and diblock, using $H = 54$ and varying surface field $\varepsilon_M \geq 0$, respectively. For the diblock we find only a few surface structures: a (structured) wetting layer (W) for $\varepsilon_M \leq 2$, spheres (S) for $\varepsilon_M = 3$, parallel cylinders ($C_\parallel$) for $4 \leq \varepsilon_M \leq 13$ and lamella (L) for $\varepsilon_M \geq 14$. With decreasing ε_M, the wetting layer increasingly adapts planar symmetry: W = S for $\varepsilon_M = 2$ and W = PL for $\varepsilon_M = 0$. The surface reconstruction $C_\parallel$ becomes connected for increasing ε_M due to the formation of interconnections between neighboring cylinders. Stable perforated lamellae with hexagonal ordering of perforations (PL) are not identified for any surface field. For $\varepsilon_M = 7$ or 8, PL-like patches are found in intermediate structures and identified (from visual inspection) as mediating structure rearrangements further away from the surfaces, but the stable surface structure is $C_\parallel$. We conclude that the exact location of the boundary between the stability regions for $C_\parallel$ and L surface structures is hard to determine using our dynamic method, as defect-removal slows down close to this boundary. We note

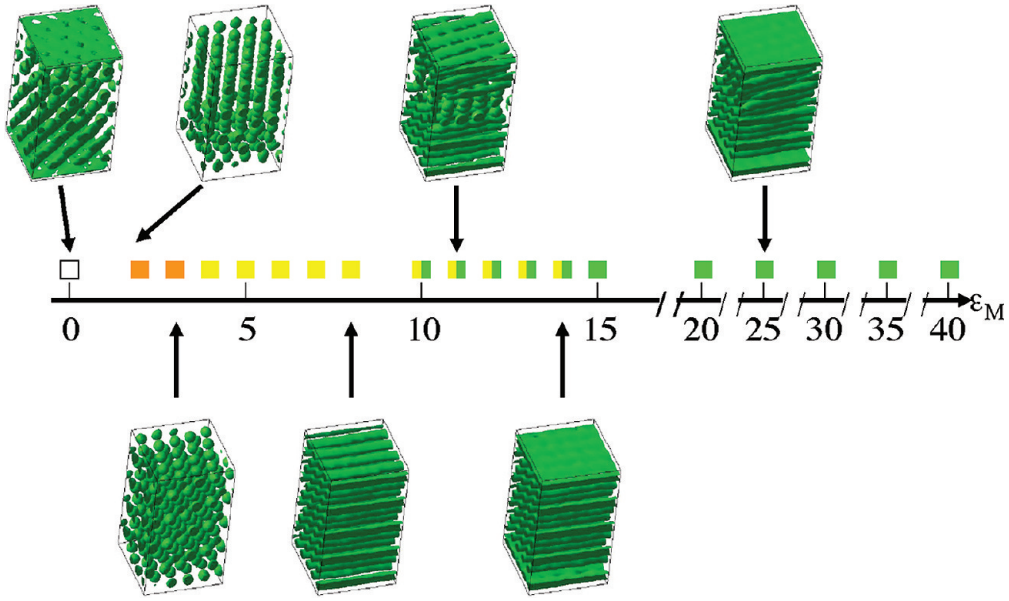

Figure 4. Stable structures in relatively thick films for the AB diblock and $\varepsilon^{di} = 6.55$. The film thickness $H = 54$ is constant and the surface field ε_M varied. The free energy was monitored during structure evolution, and calculations where extended when the free energy did not reach a constant value within 5000 steps. Representative structures are shown, and arrows indicate their location on the phase line. Colors denote the structure in the surface layers. The value used for generating the isosurfaces was the average value.

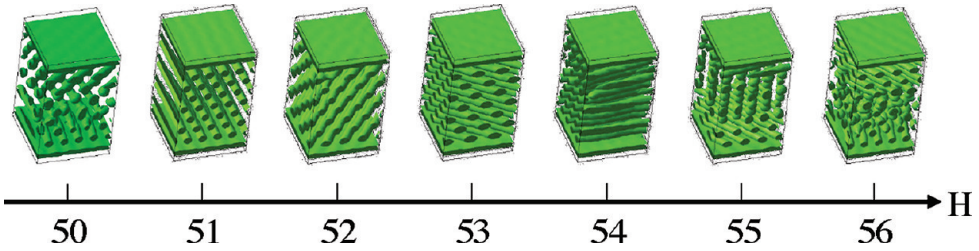

Figure 5. Stable structures for the AB diblock for varying thickness H and strong surface field $\varepsilon_M = 40$, using a standard 5000 time steps. The value used for generating the isosurfaces was the average value.

also that, even for very large surface fields $\varepsilon_M = 40$, the surface reconstruction (L) is not completely featureless along the in-plane direction, but shows (fuzzy) cylinders when imaged for very high isodensity values. For the triblock, we find: W for $\varepsilon_M \leq 2$ (either W = L or W = S), perpendicular cylinders ($C_\perp$) for $\varepsilon_M = 3$, $C_\parallel$ for $4 \leq \varepsilon_M \leq 13$ and L for $\varepsilon_M \geq 14$. Apart from the structure for $\varepsilon_M = 3$ all surface structures are equivalent to the ones found for the diblock.

In earlier studies for cylinder-forming systems,[10,11] the surface structure always converted to the bulk structure in the interior of the film, in particular hexagonally ordered cylinders aligned parallel to the film plane. Here, the structure in the interior of the film is the bulk S structure only in a small region around $\varepsilon_M = 2$ but $C_\parallel$ in most other cases. In addition, we find coexisting S/$C_\parallel$ structures (diblock, $\varepsilon_M = 0$ and 11) and even $C_\perp$ (triblock, $\varepsilon_M = 3$) through the complete film. The origin can be 2-fold. One option is that commensurability effects cannot be disregarded even in relatively thick films. In that case, the conversion from S to $C_\parallel$ in the interior of the film suggests that the mismatch changes (the system becomes more incommensurable) when surface reconstructions are formed. However, while considering the concentration profiles averaged over the two in-plane directions (not shown here), we do find some differences, but no clear indication for a distinct structure-thickness dependency of the surface layer. Another possibility is that the range of the surface field is substantially larger than in cylinder-forming systems.[49] Additional calculations for the diblock system and large surface field $\varepsilon_M = 40$ (see Figure 5) show that the structure in the interior of the film is indeed sensitive to H. For $H = 50$ (8 layers of structure) and $H = 55-56$ (9 layers of structure) the bulk structure S (in the middle of the film) is found to coexist with $C_\parallel$ (next to the surface structure). For all other H in Figure 5 we find only $C_\parallel$ in the interior. Further, we have determined the behavior for the triblock system and $H = 54$ (see Figure 6) further away from the bulk sphere/cylinder phase boundary ($\varepsilon_{AB} = 5.8$ of ref 29). For completeness, we note that this lower interaction will also change the bulk domain distance s_0, albeit only slightly. However, the absence of any structure formation for $\varepsilon_M = 3$ shows that $H = 54$ is incommensurate also for this AB interaction. In particular, the combination of lower interaction (closer to ODT) and frustration leads to a suppression of phase separation. From Figure 6, one can see that the interior $C_\parallel$ for $\varepsilon^{tri} = 5.9$ (Figure 3) transforms into mostly S (bulk-like) structures for $\varepsilon^{tri} = 5.8$, while next to L surface reconstructions $C_\parallel$ is again found. Using these findings, this complex behavior can be rationalized as follows. First, spheres are more sensitive to frustration in one direction than cylinders, because of their 3D nature and reduced deformability. Second, cylinders play a role as connectors, i.e. as intermediate between structures of increasing planar symmetry (surface reconstructions associated with large elastic chain deformations like $C_\parallel$ or L) and nonplanar symmetry (S). In particular, the results show that surface reconstruction *in combination with* frustration always induce a transition from bulk spheres to

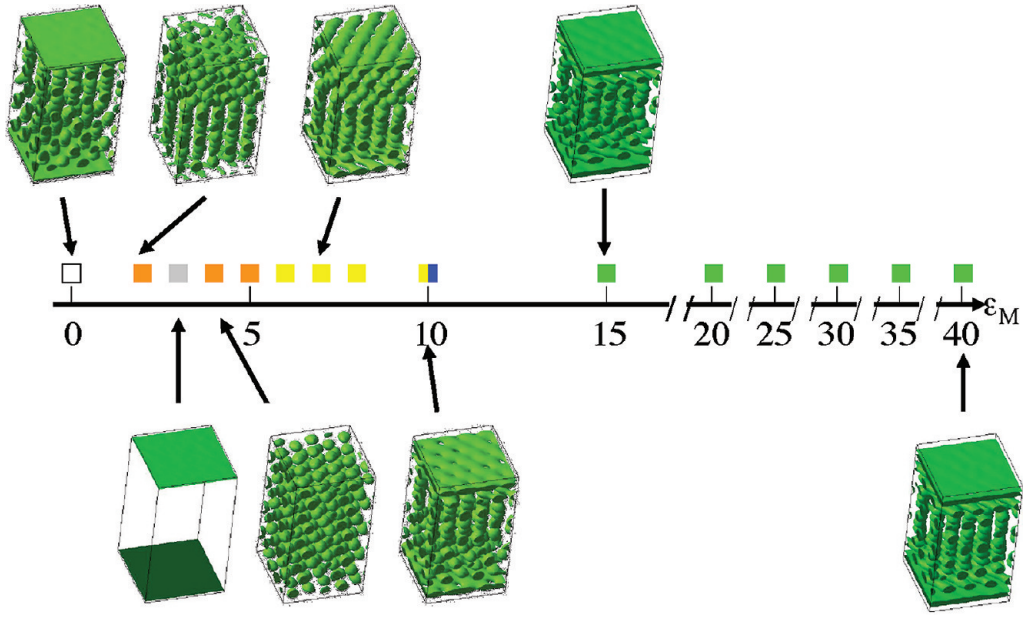

Figure 6. Stable structures for the ABA triblock and $\varepsilon_{AB} = 5.8$, slightly lower than in Figure 3. The film thickness $H = 54$ is constant and the surface field ε_M varied. The free energy was monitored during structure evolution, and calculations where extended when the free energy did not reach a constant value within 5000 steps. Representative structures are shown, and arrows indicate their location on the phase line. The value used for generating the isosurfaces was the average value.

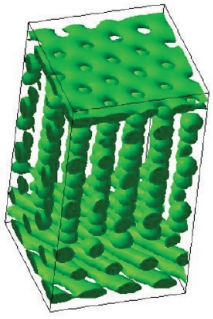

Figure 7. Representative structure for the considered AB diblock with $H = 55$ and $10 \leq \varepsilon_M \leq 15$. The shown structure is for $\varepsilon_M = 11$ and 5000 time steps. The value used for generating the isosurfaces was the average value.

cylinders in part of the film, independent of thickness. Cylinders form a deformable transition zone that resolves frustration and stabilizes the bulk S structure in the remainder of the film, i.e., deeper in the interior. This reasoning is confirmed by two additional calculation setups for the diblock. For $H = 108$ or 19 layers of structure with high surface field, $\varepsilon_M = 40$ (results not shown here), we find surface reconstructions (L) and 8 layers of spheres in the center of the film, separated by (several layers) of $C_{\parallel}$ at both sides. The distribution of the number of cylinder layers in the transition zone at both sides is asymmetric. This is an interesting finding, as the surface field is symmetric. We conclude that the asymmetry results from packing restrictions and microphase separation, that initiates some degree of randomness. In addition, we considered $H = 55$ and varying $2 < \varepsilon_M < 15$, a film thickness (9 layers) that we previously identified as more commensurable than $H = 54$. For this thickness, we identify the same type of asymmetry. While to structure in the center of the film remains mostly spherical, one surface layer shows a $S \rightarrow C_{\parallel} \rightarrow PL \rightarrow L$ transition with increasing surface field, and the other a $S \rightarrow C_{\parallel} \rightarrow L$ transition without visiting the PL phase. In Figure 7, we show a typical result for surface fields $10 \leq \varepsilon_M \leq 15$. Close to each of the surfaces *different* surface reconstructions appear: PL and $C_{\parallel}$. The PL directly connects to a layer of spheres, while the layer next to $C_{\parallel}$ contains cylinders. Each of the surface layers experiences a transition upon further increase of the surface field, from $C_{\parallel}$ to L and from PL to L, in combination with the formation of two and one adjacent layer(s) of cylinders, respectively. We therefore conclude that confinement and surface field effects can therefore in general not be decoupled for fixed H. The driving force for the formation of surface reconstructions and packing constraints in the whole film have a complex interplay. As a result, the mechanisms for surface reconstruction are nontrivial and coexisting $S/C_{\parallel}$ structures dominate the interior of films. In supported films, incommensurability will be resolved by the formation of terraces of (half) integer multiples of microdomain thickness. The results suggest that the unifying mechanisms for cylinder-forming systems are valid for sphere-forming systems on these terraces. However, even in a commensurable thickness, the interior structure (S) will be separated from the surface reconstruction by (several) layers of cylinders.

From Figures 3 and 4, we find that both the surface reconstructions and structures in the interior are not very sensitive to the particular chain architecture, AB or ABA. Only for the neutral surface fields $\varepsilon_M = 3$, where the weak repulsion of the A block levels with the entropic gain of positioning the shortest part of the chains next to the surface, we observe a clear difference between the diblock and triblock. For the triblock, spheres connect into a stable $C_{\perp}$ structure at later stages, a process that is accompanied by a significant decrease of the free energy. Lowering the AB interaction (to $\varepsilon^{tri} = 5.8$, see Figure 6) for the triblock even suppresses structure formation for this surface field value, hinting that $C_{\perp}$ results from frustration. For the equivalent diblock, S instead of $C_{\perp}$ is found to be stable and extended number of simulation TMS give only rise to defect removal, i.e., enhancing the order in the "soft crystal". The origin of this difference between diblock and triblock can be found in the entropic contribution, and is due to the conformational freedom of the triblock to form either bridges or loops. Apparently, standing cylinders are entropically favored in triblocks due to bridging.

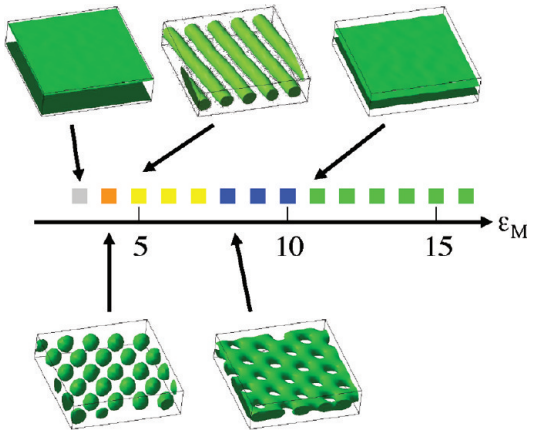

Figure 8. Stable structures in one domain thick films for the ABA triblock and $\varepsilon_{AB} = \varepsilon^{tri} = 5.9$. The film thickness $H = 7$ is constant and the surface field ε_M varied. The free energy was monitored during structure evolution, and calculations where extended when the free energy did not reach a constant value within 5000 steps. Representative structures are shown, and arrows indicate their location on the phase line. The value used for generating the isosurfaces was the average value.

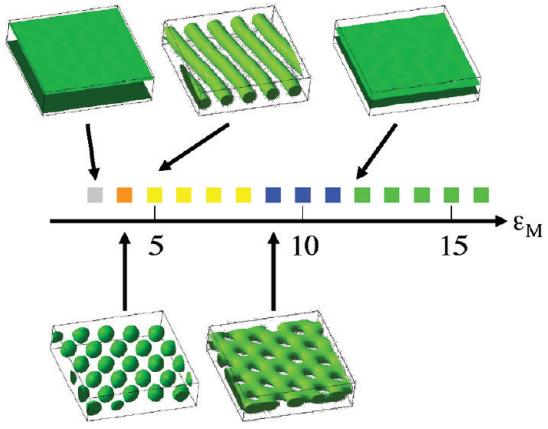

Figure 9. Stable structures in one domain thick films for the AB diblock and $\varepsilon_{AB} = \varepsilon^{di} = 6.55$. The film thickness $H = 7$ is constant and the surface field ε_M varied. The free energy was monitored during structure evolution, and calculations where extended when the free energy did not reach a constant value within 5000 steps. Representative structures are shown, and arrows indicate their location on the phase line. The value used for generating the isosurfaces was the average value.

7. One Microdomain Thick Films

Thin films of one natural domain spacing allow us to concentrate on the effect of the surface field, as modulation due to incommensurability is absent. Owing to the vicinity of the two confining surfaces, the surface fields may overlap and give rise to surface constructions for lower values of the surface field than for thicker films (interference of surface fields, see refs 10 and 11). Nevertheless, we noted great sensitivity to packing issues in the previous section. Because of the integer increments of the film thickness in our calculations, incommensurability may play a role even in very thin films. Considering both systems, we find that the spherical and cylindrical structures for $H = 6$ ($\sim s_0$ determined from bulk calculations) are somewhat compressed, indicating that the structure is frustrated. Moreover, L is already found for relatively low surface fields, i.e. $\varepsilon_M \geq 6$. For $H = 7$, this compression is resolved, and we conclude that the actual value of s_0, i.e., one microdomain in confinement, is between 6 and 7 grid spacings. The structures are shown in Figures 8 and 9, for the triblock and diblock, respectively. With increasing ε_M, we find: disorder (D), S, $C_{\parallel}$, PL, and L. The results for the diblock and

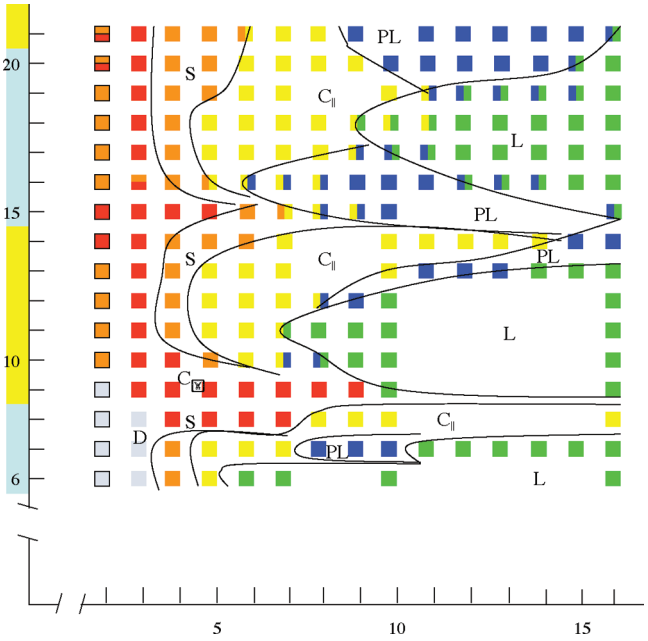

Figure 10. Diagram of stable structures for the ABA triblock and $\varepsilon_{AB} = \varepsilon^{tri} = 5.9$. Both the film thickness H (vertical axis) and the surface field ε_M (horizontal axis) were varied. The free energy was monitored during each structure evolution, and calculations where extended when the free energy did not reach a constant value within 5000 steps. Colors denote the structure in the surface layers. The boundaries of the phase regions are sketched to guide the eye. Coloring on the vertical axis indicates a change in the number of layers.

triblock are very similar, but the boundaries for PL and L surface reconstruction are shifted to slightly lower surface fields for the triblock. Naturally, the longer ABA chain will experience a larger entropic penalty due to the presence of the confining surfaces. Upon comparing cylinder- and sphere-forming ABA single domain films,[11] we find that they are very similar for larger surface fields. In particular, we find an equivalent $C_{\parallel} \rightarrow PL \rightarrow L$ transition with increasing surface field. This is not surprising, since $S \rightarrow C$ transitions under external fields were previously identified[20−22] and the surface field effect was previously identified as universal. For almost neutral surfaces, the behavior is substantially different. Since S is rotational symmetric, orientational transitions between $C_{\perp}$ and $C_{\parallel}$ are not expected. Instead, the bulk S structure is very sensitive to either frustration due to confinement or the surface field. We identify two consequences: the S-region is very small, and phase separation is even suppressed for a neutral surface field $\varepsilon_M = 3$ in strong confinement.

8. Structure Diagrams

Next, we systematically consider all films for $6 \leq H \leq 21$, i.e. one to four layers of structure. Since we are interested in surface structures, we again focus on part of the diagram ($3 \leq \varepsilon_M \leq 16$) where an A-rich wetting layer W is absent. Figures 10 and 11 display surface structures for both triblock and diblock, respectively. From the diagrams, it is again clear that a simple explanation, i.e., based on largely decoupled commensurability and surface field effects, is not accurate for sphere-forming systems. For instance, the nesting of structures with increasing planar symmetry in cylinder-forming systems is not observed here. As discussed before, one should instead consider the connectivity of the surface structure to the interior of the film. This gives rise to a natural separation of the diagram into one or two layers of structure, i.e., only surface structure, and more layers of structure. On the basis of the images and the value for one domain thick films $s_0 \approx 7$, we determine the commensurate

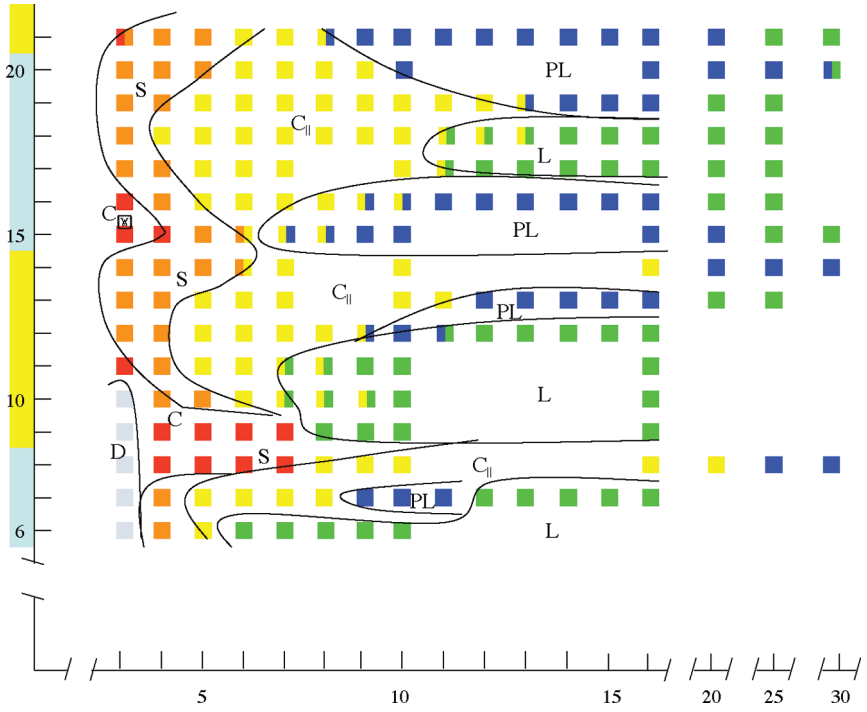

Figure 11. Diagram of stable structures for the AB diblock and $\varepsilon_{AB} = \varepsilon^{di} = 6.55$. Both the film thickness H (vertical axis) and the surface field ε_M (horizontal axis) were varied. The free energy was monitored during each structure evolution, and calculations where extended when the free energy did not reach a constant value within 5000 steps. Colors denote the structure in the surface layers. The boundaries of the phase regions are sketched to guide the eye. Coloring on the vertical axis indicates a change in the number of layers.

thicknesses as $H = 14$ ($\approx 2s_0$, two domains) and $H = 20$ ($\approx 3s_0$, three domains). We see that close to these values, for $H = 9$ and 15, one layer of structure is added. For $H = 21$, the diblock forms four layers over the whole range, but for the triblock the interior of the film is $C_\perp$ for $12 \leq \varepsilon_M \leq 16$ (three layers). We therefore conclude in general that chain compression is much more favored over stretching in these systems. In addition, the bulk S structure is found only in a small part of the diagram for low surface fields, indicating again the reduced stability of the bulk structure against confinement frustration and surface field when compared to cylinder-forming systems.

8.1. One and Two Layers of Structure. For one and two layers of structure, we find evidence for interference of the two surface fields (of the bottom and the top surface). Comparing the commensurate thickness $H = 14$ and 7, we find that the surface field required to induce PL and L surface reconstructions is strongly reduced for the thinner film ($H = 7$). In addition, both S and $C_\parallel$ regions extend to higher values of ε_M and are broader, indicating that the surface field increases more gradually for $H = 14$. The effect is even amplified when compared to the cylinder-forming systems, where the shift of the PL and L boundaries between the first and second layer was found to be $\Delta\varepsilon = 1-3$ kJ/mol.[10,11] Here, the shift for the PL boundary in the triblock is 7 kJ/mol, and others are even larger.

For very incommensurate films ($H = 9-11$), the PL phase is completely absent as an intermediate between $C_\parallel$ and L. Instead, for increasing surface field L forms either from $C_\perp$ ($H = 9$) or $C_\parallel$ ($H = 10-11$). At the boundary of the L region, $C_\perp$ has a specific "diabolo" shape, i.e., thinned in the middle and extended at the two ends. For $H = 10-11$, L is often found to coexist with $C_\parallel$ at its boundary, in the form of the earlier observed connected cylinders. Closer to the commensurate situation ($H = 12-13$), PL is identified as an intermediate between $C_\parallel$ and L, and its stability region broadens with increasing H.

The situation for $H = 8$ is special, as the film is too thin to form two layers of structure, while chain stretching is required to fill interstitial space between the two confining surfaces. For low surface fields, the frustration can be resolved by the formation of $C_\perp$. For larger surface fields, $C_\perp$ merges into elongated $C_\parallel$. The stability of this phase is remarkable, and ranges to $\varepsilon_M > 16$ for both diblock and triblock. For the diblock, we determined the phase boundary for $C_\parallel \rightarrow$ PL transition as $\varepsilon_M \approx 25$. We conclude that much higher surface fields are required to induce surface reconstructions, due to the unfavored chain stretching in these structures.

For neutral surfaces, strong confinement suppresses phase segregation, and gives rise to a disordered phase with no well-defined microdomain structure, however, with the A and B blocks still slightly segregated. This disordered phase extends to higher H for the diblock than for the triblock. Upon increasing H, $C_\perp$ (triblock) or S (diblock) is formed. Only for the most incommensurate $H = 11$, $C_\perp$ is found for the diblock due to frustration.

8.2. More Layers of Structure. The most striking feature for films of $H \geq 15$ is the prominent PL regions, that extends well into the lower surface field range. First we focus on the connection between the surface structure and the interior of the film. We find that $C_\parallel$, PL, and L surface reconstructions combine with $C_\parallel$, S, and $C_\parallel$ in the interior of the film, respectively. Keeping in mind that the PL phase can be regarded as an array of touching spheres,[50] we conclude that these combinations require the least amount of chain stretching. There are a few exceptions. For $H = 19$, the situation is less clear. While $C_\parallel$ is found in the interior of the film, the surface structure for increasing surface field is either a $C_\parallel$/PL or PL/L coexistence depending on the isosurface value used for imaging. For $H = 20$ and $6 \leq \varepsilon_M \leq 9$ (diblock) and $H = 21$ and $\varepsilon_M = 6$ (triblock) $C_\parallel$ surface reconstructions combine with S (one or two layers) in the interior of the film. In line

with the earlier observations, we conclude that the formation of PL surface reconstructions is suppressed in very incommensurate films ($H = 17-18$), where the $C_{\parallel}$-region is considerably extended into the large surface field range. Closer to the commensurate situation ($H = 15-16$ and $19-21$), PL is found as an intermediate between $C_{\parallel}$ and L. This PL exists in combination with compressed S ($H = 15-16$), $C_{\parallel}$ ($H = 19$), S ($H = 20$) and either two layers of compressed S or $C_{\perp}$ ($H = 21$). We identify two important factors: first, increasing the surface field gives rise to structures with an increasing planar symmetry, i.e. $C_{\parallel}$, PL, and L, just like for cylinder-forming structures. Nevertheless, the trade-off between surface energy and conformational entropy, i.e. the chain deformation that is required to fill the interstitial space, is much more substantial. Apparently, when the interstitial space between the two confining surfaces requires moderate chain stretching/compression, the formation of PL surface reconstructions in combination with (modulated) bulk structure S in the interior is promoted. In particular, PL is stable in thicker films from about the same surface field as PL for $H = 7$, showing the complex interplay of surface field and confinement, and this PL region is considerably extended. When the required chain deformation become too large, i.e. for $H = 17-18$, $C_{\parallel}$ is stabilized and the surface structure transforms into L for increasing surface field without visiting PL.

For neutral surfaces, again $C_{\perp}$ (triblock) or S (diblock) is formed. Only when a layer is added, $H = 15-16$ and 21, $C_{\perp}$ is formed for the diblock due to the frustration.

9. Comparison of Diblock and Triblock

In the previous sections, we have noted several differences between sphere-forming diblock and triblock confined in thin films. The main difference is in the behavior for neutral films. Here, confinement induces the formation of perpendicular cylinders $C_{\perp}$, independent of the film thickness, for the triblock. The diblock forms spheres S, apart from films with H where chains are slightly extended. In this case, $C_{\perp}$ is stabilized also for non-neutral films in both systems. Furthermore, the stability of both $C_{\parallel}$ and PL surface reconstructions in films of up to 4 layers of structure is reduced in favor of L for the triblock in comparison to the diblock. For very thick films ($H = 54$), where PL was absent, we observed no difference, however, apart from the behavior for a neutral surface field.

10. Free Energy Considerations

We have carefully avoided the notion of phase diagrams for Figures 10 and 11. All film structures in the previous sections have been obtained by minimization of the free energy (1) using diffusive dynamics (2). Stable structures, corresponding to plateau values of the free energy within finite simulation time, are therefore not necessarily equilibrium structures, but can also represent long-living metastable states. The benefit of our dynamic method is that the experimental structure and structure evolution can be reproduced rather well.[28] Static methods, like self-consistent field theory (SCFT) adapted for confinement, lack this kinetic component but are in general better suited for extracting accurate information about the equilibrium phase behavior. Nevertheless, the free energy (1) can be useful for the analysis of our results. We have previously shown for cylinder-forming systems that the free energy for slits provides information on terrace formation in supported films via a common tangent procedure.[37] To promote clarity of presentation here, we postpone such an analysis to future publications where we will focus on a comparison to detailed experimental observations. Here, we only shortly illustrate how the free energies for varying surface field can be used to extract additional information.[51] In

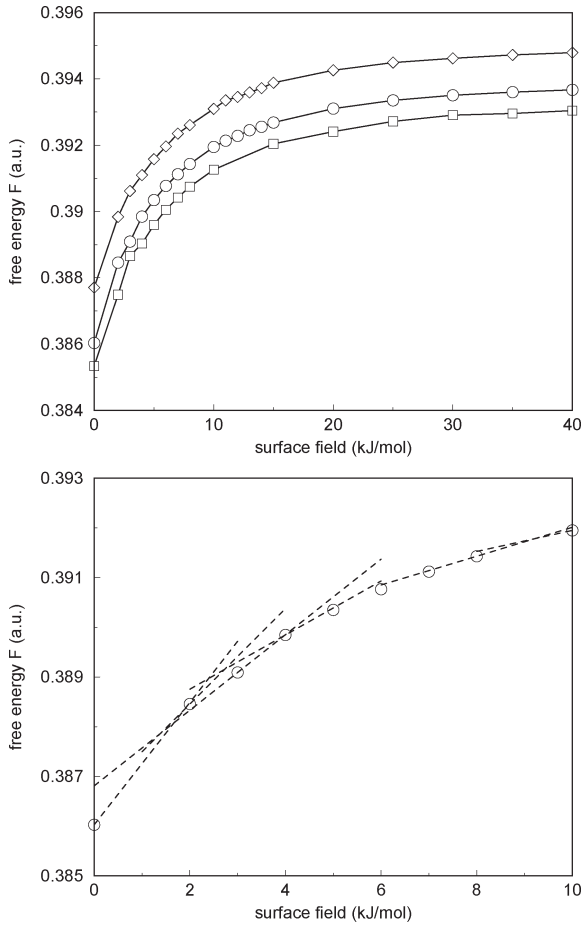

Figure 12. Top: Free energy per unit volume for the stable structures in thick films with $H = 54$. The surface field ε_M is varied on the horizontal axis. The free energy F for the ABA structures in Figure 3 ($\varepsilon_{AB} = 5.9$, circles) is compared to the free energy for the AB structures in Figure 4 ($\varepsilon_{AB} = 6.55$, diamonds) and the ABA structures in Figure 6 ($\varepsilon_{AB} = 5.8$, squares) after translation. The translation, $F(\varepsilon_M) + \overline{F}$, is for visualization purposes only. The fixed $\overline{F}$ is - 0.04 (diamonds) and 0.005 (squares), respectively. Solid lines connect calculated free energies to guide the eye. Bottom: (circles) free energies for the ABA structures in Figure 3, and (dashed straight lines) extrapolated free energies, obtained by using the stable structures in $\varepsilon_M = 0$, 2, 3, 4, 8, and 10 of Figure 3 in the determination of free energies for different surface fields.

Figure 12 (top) we have plotted the free energy F, normalized by the occupied volume, for the stable structures in Figure 3 and varying surface field. The system is the ABA triblock for $H = 54$. The shape of this free energy curve is typical, which we quantify by also plotting the free energies for the AB structures in Figure 4 ($H = 54$) and the ABA structures in Figure 6 ($H = 54$ and $\varepsilon_{AB} = 5.8$) in the same figure. To enable a visual comparison, we have applied the affine translation $F(\varepsilon_M) + \overline{F}$ to these curves, with $\overline{F}$ appropriately chosen.

Next, we focus on the free energy curve corresponding to the structures in Figure 3, and find that $F(\varepsilon_M)$ approaches a straight line for strong surface fields. A linear relation is the hallmark of structure that does not change with increasing surface field.[51] With decreasing surface field, the structure changes and the free energy decreases nonlinearly. From Figure 3, one can observe that the structure in the interior of the film does not significantly change until $\varepsilon_M = 4$, so we conclude that the principal contribution is due to the surface-field induced chain deformation, i.e., the $L \rightarrow C_{\parallel}$ transition via hole formation in the layer adjacent to the surfaces. Both a detailed analysis (not shown here) and the absence of kinks in this range, see Figure 12, suggest that this is not a first order transition. In particular, we analyzed by

extrapolating the free energy F for all stable structures in Figure 3 to other surface fields, a procedure that results in straight lines associated with each structure.[51] This procedure is illustrated in Figure 12 (bottom) for the range $0 \leq \varepsilon_M \leq 10$, and indicates that all simulated structures but one are equilibrium structures. Only the structure for $\varepsilon_M = 2$ seems kinetically frozen. Visual inspection of this structure (after 25000 time steps, see Figure 3) reveals two perfectly packed clusters of spheres, and a (defected) grain boundary that originates from an orientational mismatch between both clusters. Considering the evolution pathway, we find spheres on an irregular lattice already in the early stages. The next stage, the formation of two perfect lattices and a complex grain boundary, is very slow, and involves structure reorganization via propagation and removal of defects. Sluggish dynamics, or a small thermodynamic driving force, is also apparent in the slightly defected $C_\perp$ structure for $\varepsilon_M = 3$, which is obtained from irregular S after long simulation (20000 time steps). Although each defect represents only a minute contribution to the free energy, defect removal can in some cases be identified as tiny steps in the free energy evolution. In this particular case, the free energies for several structure-types are very comparable (see Figure 12), and we conclude that our procedure is not decisive. Improved accuracy can be obtained by considering perfect structures, e.g., using SCFT, but we note that the determination of equilibrium phase behavior was no purpose here. In most cases, for instance in the common tangent approach mentioned above, the free energy differences are much larger and our procedure suffices.

11. Comparison to Existing Studies

As far as we are aware of, confinement-induced transitions in sphere-forming block copolymers to nonspherical morphologies were only studied by theoretical means.[23−25] Pereira[23] used a theoretical analysis in the strong-segregation limit (SSL) to show that a sphere-to-cylinder transition is possible when strain is applied. He concluded that such a transition is also found in very thin films as a result of the rather high strains that arise from incommensurability, i.e. the mismatch between the natural domain spacing and the film thickness. For thicker films, spheres should be stable but their shape should be oval. We note that our systems are in the weak segregation regime. Tan et al.[24,25] used Landau−Brazovskii theory in the weak-segregation limit (single mode approximation). In their first study,[24] they concentrated on the surface field effect and found that the surface structure, i.e. the layer closest to the confining surface, shows a S → $C_\parallel$ → L transition with increasing surface field, although they denote the latter phases as cylinder-like and lamella-like. In addition, they found a $C_\parallel$ → S (for a $C_\parallel$ surface reconstruction) or L → $C_\parallel$ → S (for a L surface reconstruction) in the direction perpendicular to the confining surface, i.e. toward the interior of the film. These results are in excellent agreement with our findings for thicker films (see section 6). In their follow-up[25] the same group considered the film thickness as an additional parameter for two different surface field strengths. For these surface fields, they find (undulating) L surface reconstructions for *all* considered thicknesses. We note that, due to restrictions in their model and the parameter-set, details of the interplay between the surface field and incommensurability were not clarified.

The effect of chain architecture in confined cylinder- and lamellae-forming AB and ABA systems was studied both by experiments and SCFT.[52] The SCFT calculations focused solely on the surface field effect, in particular the orientation for increasing repulsion between the surface and the A block. They always considered an optimal or commensurate film thickness for parallel orientations. For lamellae-forming systems (50/50 AB and 25/50/25 ABA) it was found that the chain architecture is important due to the conformational penalty present in parallel structures, a penalty that is associated with triblock looping in the surface layer. As a result, SCFT locates the transition from perpendicular to parallel structures at a much higher surface field for triblocks when compared to the diblock, where looping is no issue. Hence, for block copolymers with a relatively small difference in surface energy $\Delta\gamma$, diblocks may form a parallel structure while equivalent triblocks form a perpendicular structure, a finding that was supported by the experiments. For cylinder-forming triblocks (37/25/38 ABA, cylinders of the central B block) the stability region for the perpendicular structures was found to be rather small. Above this threshold surface field, the competition between surface reconstruction and elastic chain deformation gives rise to a B-rich wetting layer, where the triblocks are again in the looping conformation. We note that our results are complementary rather than directly comparable to this earlier study. First, a comparison between the surface-field-induced transition of perpendicular *cylinders* to a B-rich wetting layer for an equivalent diblock system was not made in Khanna et al. Second, the formation of any parallel or perpendicular structure in sphere-forming systems is accompanied by alteration of the bulk structure, which does not process a symmetry axis. Moreover, due to weaker phase segregation, the contribution of elastic chain deformations is reduced. Third, the structures in this study are calculated by a diffusive procedure that can produce long-living metastable states, just like in experiments. The SCFT in Khanna et al. is static. Finally, and most important, the SCFT study[52] focused on looping chain conformations, by virtue of the chosen experimental ABA triblock system. The shortest cylinder-forming block in the ABA system in Khanna et al. is the center B block, and chain conformations that bridge between different cylinders are therefore ruled out. In our study, we find that bridging conformations apparently stabilize $C_\perp$ for the triblock in neutral conditions, whereas the diblock forms the bulk S structure. Note that the neutral surface field is shifted to positive values, due to the entropic gain of having the shortest block close to the surface in case of equal surface tension. In addition, we have not considered the part of the diagram where the surface is wet by the shortest, sphere-forming block. One should keep in mind that our triblock model for $\varepsilon_{AB} = 6.5$ was earlier used to model SBS, and that the formation of a glassy polystyrene (the A block) wetting layer prevents imaging of the deeper structure in experimental conditions. In our sphere-forming triblock system, looping and bridging is simultaneously present in (perforated) lamellae that are formed due to surface reconstruction and the connecting structure in the interior of the film. Nevertheless, our thin film results for the sphere-forming di- and triblock are qualitatively similar for non-neutral conditions. Our results only indicate that it is a complex effect, and that the formation of the parallel PL and L structures is slightly enhanced in the triblock when compared to the diblock. Since our DDFT free energy functional is the same as in the SCFT used in Khanna et al.,[52] we believe that our study provides valuable additional information.

After the present work was finished, we learned about the very recent publication of Tan et al.,[53] where the film thickness H and $\varepsilon_M = -\varepsilon^0_{AM}/\nu kT$ were systematically varied for a sphere-forming A_8B_2 diblock system confined between two flat surfaces. We note that the kT factor is accidentally omitted in their paper, and that it remains unclear whether $\chi_{AM} = \varepsilon^0_{AM}/\nu kT$ or ε^0_{AM} itself was varied. We assume that the authors varied the latter. They used a commercially available implementation of our DDFT method, also known as MesoDyn, to determine (meta)stable structures. We conclude that the results of ref 53 support as well as complement our results for the diblock. Just like in our diblock system, surface reconstructions like a wetting layer, parallel cylinders, perforated lamellae and lamellae were found for

increasing surface field. In addition, a rather compressed region of stable spheres S is found in the vicinity of neutral conditions, and perpendicular cylinders extend to higher surface fields in thin incommensurate films. However, $C_\perp$ instead of S was observed for neutral conditions ($\varepsilon_M = 5$, see ref 53), indifferent of the film thickness. In addition, confinement was shown to have no observable effect in films of three or more layers of structure. For these film thickness, only the surface reconstructions vary with increasing surface field, and the interior of the film always adapted a spherical structure. This result clearly contrasts our finding for the diblock, where the range of the surface field in general extends beyond the surface layer. We note, however, that also earlier studies of the same authors, based on Landau−Brazovskii theory in the weak-segregation limit,[24,25] concluded that nonspherical structures are stable for several layers into the interior of the film. Because of the absence of quantitative data in the study of ref.[53], it is hard to draw conclusions about the origin of these differences. Since we also want to refrain from speculating, we only mention that the fractions f of the sphere-forming block are reasonably different: $f = 1/5$ for ref 53 and $f = 1/3$ in our case. Their bulk diblock system clearly resides in a different part of the phase diagram, where, in addition, spheres are stable in a much broader χ or T range.[39] Consequently, one may expect that the increased elastic energy costs, associated with deforming part of the microstructure from spheres into cylinders, prevent the formation of the earlier mentioned cylindrical zone that connects surface structures and the interior of the film. Since we cannot confirm this based on existing data, we only conclude that the results of ref 53 are complementary to our study.

12. Conclusions

We have used dynamic density functional theory (DDFT) to study structure formation in sphere-forming AB and ABA block copolymer systems confined between two parallel solid plates (a slit). We have carefully determined Flory−Huggins interaction parameters that give rise to equivalent systems in bulk. Consequently, stable structures for both systems have been determined in a broad range of surface fields and film thickness. The considered ABA system previously showed a sphere-to-cylinder transition upon application of a strong enough external electric field.[29]

In line with earlier studies for lamellae- and cylinder-forming systems, we have concentrated on the effects of the two factors that are simultaneously active in a thin film situation: the surface field and confinement, i.e., the film thickness. In case of a mismatch between the film thickness and the natural domain thickness, or incommensurability, the structure formation is modulated by confinement effects. In cylinder-forming systems, the *range* of the surface field was found to be roughly one domain spacing,[10,11] giving rise to the concept of decoupling: the structure in the interior of the film is fairly independent of the nature of the surface reconstruction, for films of commensurate thickness. Our present results reveal the complex interplay of both factors in spherical systems. A general finding is that the stability of spheres is considerably reduced compared to cylinders in cylinder-forming systems, both in the surface layer and in the interior of the film. This is a first indication of their reduced stability to deformation. We identified several surface reconstructions similar to the ones observed in cylinder-forming block copolymers: a wetting layer (W), parallel cylinders ($C_\parallel$), perforated lamellae (PL), and lamellae (L). However, in sphere-forming systems, the earlier mentioned concept of decoupling is frustrated by connectivity, in particular restrictions to the chain conformations that connect the structure in the surface layer and the interior of the film. As a result, the apparent *range* of the surface field is surface-structure dependent, and nonbulk structures can extend into the interior of the film. In particular, and in full agreement with earlier theoretical work,[24,25] W, $C_\parallel$, and L surface reconstruction are accompanied by several layers containing *cylindrical* structures, adjacent to the surface reconstructions. These cylindrical layers constitute a deformable transition zone between the surface reconstructions and the structures in the remainder of the slit, and the thickness of this zone at both sides of the slit is generally different. Since connectivity between bulk spheres and the remaining surface reconstruction, PL, is not an issue, the cylindrical transition zone is absent in this case. Surface field additivity[11] is observed for one- or two-layered films, i.e., for surface structure only. Confinement modulates these effects in a very nontrivial way. For very incommensurate films, surface reconstructions transform with increasing surface field from $C_\parallel$ to L, without visiting the PL phase. For slightly incommensurate films, the PL surface reconstruction is also found as an intermediate. Confinement and surface field effects are in general coupled, and packing frustrations in the whole film may even stabilize *different* surface reconstructions at each side of the slit. The sensitivity to incommensurability extends to much thicker films than in cylinder-forming systems, and the range of the surface field is increased.

The chain architecture, AB or ABA, plays an important role only for neutral films. Here, the entropic effect is balanced by the energetic repulsion for the shortest part of the chain. For neutral films, a new structure, film-spanning perpendicular cylinders or $C_\perp$, is stable for any thickness in the triblock system, while layers of spheres (S) are found for the diblock. The only exception in the diblock system is for a film thickness when one layer of structure is added, where restrictions to elastic chain deformation gives rise to the formation of $C_\perp$. Apparently, bridging chain conformations parallel to the confining surfaces in the triblock stabilize $C_\perp$ for neutral films. For preferential and relatively thin films, the locations of the phase-boundaries shift to (slightly) lower surface field values for the triblock when compared to the diblock. For thicker preferential films, we observe no differences.

We note that the studies considering this system are fairly limited, and that the majority of these studies is focused on spherical packing and packing-transitions in films of different thickness. The experiments referred to in the introduction[26] could serve as a benchmark system for the detailed validation of our findings, and serve as a starting point for further theoretical study. We leave a detailed comparison for future publications.

Acknowledgment. Supercomputer time for GJAS is provided by a grant of the Stichting Nationale Computerfaciliteiten (NCF). The simulations were performed at the Huygens supercomputer at SARA (Amsterdam). The authors thank E. Thomas for providing information on the experimental findings of K. E. Sohn.

References and Notes

(1) Bates, F. S.; Fredrickson, G. H. *Annu. Rev. Phys. Chem.* **1990**, *41*, 525.Hamley, I. W. *The Physics of Block Copolymers*; Oxford University Press: Oxford, U.K., 1998).
(2) For reviews, see: Matsen, M. W. *Curr. Opin. Colloid Interface Sci.* **1998**, *3*, 40. Binder, K. *Adv. Polym. Sci.* **1999**, *138*, 1. Fasolka, M. J.; Mayes, A. M. *Annu. Rev. Mater. Res.* **2001**, *31*, 323.
(3) Rehse, N.; et al. *Phys. Rev. Lett.* **2001**, *87*, 035505.
(4) Karim, A.; et al. *J. Chem. Phys.* **1994**, *100*, 1620.
(5) Radzilowski, L. H.; Carvalho, B. L.; Thomas, E. L. *J. Polym. Sci., Part B: Polym. Phys.* **1996**, *34*, 3081.
(6) Konrad, M.; et al. *Macromolecules* **2000**, *33*, 5518.
(7) Harrison, Ch.; et al. *Macromolecules* **1998**, *31*, 2185. *Polymer* **1998** *30*, 2733.
(8) Zhang, Q.; et al. *Macromolecules* **2000**, *33*, 9561.
(9) Wang, Q.; Nealy, P. F.; de Pablo, J. J. *Macromolecules* **2001**, *34*, 3458.

(10) Knoll, A.; Horvat, A.; Lyakhova, K. S.; Krausch, G.; Sevink, G. J. A.; Zvelindovsky, A. V.; Magerle, R. *Phys. Rev. Lett.* **2002**, *89*, 035501.
(11) Horvat, A.; Lyakhova, K. S.; Sevink, G. J. A.; Zvelindovsky, A. V.; Magerle, R. *J. Phys. Chem.* **2004**, *120*, 1117–1126.
(12) Park, I.; Park, S.; Park, H-W.; Chang, T.; Yang, H.; Ryu, C. Y. *Macromolecules* **2006**, *39*, 315–318.
(13) Henkee, C. S.; et al. *J. Mater. Sci* **1988**, *23*, 1685.
(14) Yokoyama, H.; Mayes, T. E.; Kramer, E. L. *Macromolecules* **2000**, *33*, 1888.
(15) Stein, G. E.; Kramer, E. J.; Li, X. F.; Wang, J. *Macromolecules* **2007**, *40*, 2453.
(16) Yokoyama, H.; Kramer, E. J.; Rafailovich, M. H.; Sokolov, J.; Schwarz, S. A. *Macromolecules* **1998**, *31*, 8826.
(17) Segalman, R. A.; Hexemer, A.; Kramer, E. J. *Phys. Rev. Lett.* **2003**, *91*, 158302.
(18) Stein, G. E.; Lee, W. B.; Fredrickson, G. H.; Kramer, E. J.; Li, X.; Wang, J. *Macromolecules* **2007**, *40*, 5791.
(19) Stein, G. E.; Cochran, E. W.; Katsov, K.; Fredrickson, G. H.; Kramer, E. J.; Li, X.; Wang, J. *Phys. Rev. Lett.* **2007**, *98*, 158302.
(20) Tsori, Y.; Tournilhac, F.; Andelman, D.; Leibler, L. *Phys. Rev. Lett.* **2003**, *90*, 145504.
(21) Xu, T.; Zvelindovsky, A. V.; Sevink, G. J. A.; Gang, O.; Ocko, B.; Zhu, Y. Q.; Gido, S. P.; Russell, T. P. *Macromolecules* **2004**, *37*, 6980.
(22) Zvelindovsky, A. V.; Sevink, G. J. A.; Lyakhova, K. S.; Altevogt, P. *Macromol. Theory Simul.* **2004**, *13*, 140.
(23) Pereira, G. G. *Macromolecules* **2004**, *37*, 1611.
(24) Tan, H. G.; Yan, D. D.; Shi, A. C. *Macromolecules* **2004**, *37*, 9646.
(25) Tan, H. G.; Song, Q. G.; Yang, S.; Yan, D. D.; Shi, A. C. *Macromol. Theor. Simul* **2008**, *17*, 45.
(26) Sohn, K. E. Ph.D. Thesis, **2008**.
(27) Lyakhova, K. S.; Sevink, G. J. A.; Zvelindovsky, A. V.; Horvat, A.; Magerle, R. *J. Phys. Chem.* **2004**, *120*, 1127–1137.
(28) Knoll, A.; Lyakhova, K. S.; Horvat, A.; Krausch, G.; Sevink, G. J. A.; Zvelindovsky, A. V.; Magerle, R. *Nature Mat.* **2004**, *3*, 886–890.
(29) Lyakhova, K. S.; Horvat, A.; Zvelindovsky, A. V.; Sevink, G. J. A. *Langmuir* **2006**, *22*, 5848–5855.
(30) Horvat, A.; Knoll, A.; Krausch, G.; Tsarkova, L.; Lyakhova, K. S.; Sevink, G. J. A.; Zvelindovsky, A. V.; Magerle, R. *Macromolecules* **2007**, *40*, 6930–6939.
(31) Tsarkova, L.; Horvat, A.; Krausch, G.; Zvelindovsky, A. V.; Sevink, G. J. A.; Magerle, R. *Langmuir* **2006**, *22*, 8089–8095.
(32) Horvat, A.; Sevink, G. J. A.; Zvelindovsky, A. V.; Krekhov, A.; Tsarkova, L. *ACS Nano* **2008**, *2*, 1143–1152.
(33) Sevink, G. J. A.; Zvelindovsky, A. V.; van Vlimmeren, B. A. C.; Maurits, N. M.; Fraaije, J. G. E. M. *J. Chem. Phys.* **1999**, *110*, 2250.
(34) Matsen, M. W. *J. Chem. Phys.* **1997**, *106*, 7781.
(35) Fraaije, J. G. E. M.; van Vlimmeren, B. A. C.; Maurits, N. M.; Postma, M.; Evers, O. A.; Hoffmann, C.; Altevogt, P.; Goldbeck-Wood, G. *J. Chem. Phys.* **1997**, *106*, 4260.
(36) van Vlimmeren, B. A. C.; Maurits, N. M.; Zvelindovsky, A. V.; Sevink, G. J. A.; Fraaije, J. G. E. M. *Macromolecules* **1999**, *32*, 646.
(37) Huinink, H. P.; et al. *J. Chem. Phys.* **2000**, *112*, 2452.
(38) Sevink, G. J. A.; Zvelindovsky, A. V. *J. Chem. Phys.* **2004**, *121*, 3864.
(39) Matsen, M. W.; Bates, F. S. *Macromolecules* **1996**, *29*, 1091.
(40) Fredrickson, G. F. *Macromolecules* **1987**, *20*, 2035.
(41) Miao, B.; Yan, D.; Han, C. C. *J. Chem. Phys.* **2006**, *124*, 144902.
(42) Leibler, L. *Macromolecules* **1980**, *13*, 1602.
(43) Thomas, E. L.; et al. *Macromolecules* **1987**, *20*, 2934.
(44) Thomas, E. L.; et al. *Nature* (*London*) **1988**, *334*, 598.
(45) Matsen, M. W. *J. Phys.: Condens. Matter* **2002**, *14*, R21.
(46) Honda, T.; Kawakatsu, T. *Macromolecules* **2006**, *39*, 2340.
(47) Maurits, N. M.; et al. *Comput. Theor. Polym. Sci.* **1996**, *6*, 1.
(48) Drolet, F.; Fredrickson, G. H. *Phys. Rev. Lett.* **1999**, *83*, 4317.
(49) Huinink, H. P.; et al. *Macromolecules* **2001**, *34*, 5325.
(50) Fogden, A. S.; Stenkula, M.; Fairhurst, C. E.; Holmes, M. C.; Leaver, M. S. *Prog. Colloid Polym. Sci.* **1998**, *108*, 129.
(51) Sevink, G. J. A.; Zvelindovsky, A. V. *J. Chem. Phys.* **2008**, *128*, 084901.
(52) Khanna, V.; Cochran, E. W.; Hexemer, A.; Stein, G. E.; Fredrickson, G. H.; Kramer, E. J.; Li, X.; Wang, J.; Hahn, S. F. *Macromolecules* **2006**, *39*, 9346.
(53) Tan, H.; Song, Q.; Niu, X.; Wang, Z.; Gao, W.; Yan, D. *J. Chem. Phys.* **2009**, *130*, 214901.